ResearchGate

See discussions, stats, and author profiles for this publication at: https://www.researchgate.net/publication/263952269

Evidence of Phonon-Assisted Auger Recombination and Multiple Exciton Generation in Semiconductor Quantum Dots Revealed by Temperature-Dependent Phonon Dynamics

ARTICLE *in* JOURNAL OF PHYSICAL CHEMISTRY LETTERS · DECEMBER 2013

Impact Factor: 7.46 · DOI: 10.1021/jz402305r

CITATIONS
6

READS
33

3 AUTHORS:

Kim Hyeon-Deuk
Kyoto University
33 PUBLICATIONS **378** CITATIONS
SEE PROFILE

Yoichi Kobayashi
Aoyama Gakuin University
33 PUBLICATIONS **147** CITATIONS
SEE PROFILE

Naoto Tamai
Baiko Jo Gakuin University
188 PUBLICATIONS **5,873** CITATIONS
SEE PROFILE

Available from: Kim Hyeon-Deuk
Retrieved on: 29 January 2016

THE JOURNAL OF PHYSICAL CHEMISTRY Letters

Letter

pubs.acs.org/JPCL

Evidence of Phonon-Assisted Auger Recombination and Multiple Exciton Generation in Semiconductor Quantum Dots Revealed by Temperature-Dependent Phonon Dynamics

Kim Hyeon-Deuk*

Department of Chemistry, Kyoto University, Kyoto, 606-8502, Japan

Japan Science and Technology Agency, PRESTO, 4-1-8 Honcho, Kawaguchi, Saitama, 332-0012, Japan

Yoichi Kobayashi

Department of Chemistry, Aoyama Gakuin University, 5-10-1 Fuchinobe, Chuo-ku, Sagamihara-shi, Kanagawa, 252-5258, Japan

Naoto Tamai

Department of Chemistry, School of Science and Technology, Kwansei Gakuin University, 2-1 Gakuen, Sanda, Hyogo, 669-1337, Japan

Supporting Information

ABSTRACT: Auger processes, multiple exciton generation, and Auger recombination, provide and disturb a potential route to increase solar cell efficiencies by creating multiple charge carriers, respectively. Physical mechanisms of the Auger processes can be deduced from the temperature dependence. Our real-time *ab initio* simulation found logarithmic temperature dependence of the Auger rates in semiconductor quantum dots (QDs), which agrees well with the recent experimental observations. This anomalous temperature dependence is not only determined by static electronic structures of the QDs depending on temperature, but also attributed to dynamical electron−phonon couplings, directly demonstrating that the Auger processes are actually induced by the electron−phonon couplings and can be controlled by phonon modes. Our findings suggest that high-frequency and broad phonon modes of a QD including the surface ligands dictate efficient Auger dynamics in a QD.

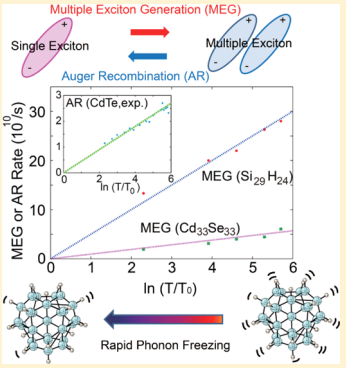

SECTION: Physical Processes in Nanomaterials and Nanostructures

The solar spectrum extends over a broad range of energies, and in most photovoltaic materials, high-energy excitations rapidly relax to the lowest excited state at the red end of the spectrum by interaction with phonons.[1] Thus, significant amounts of solar power are lost to heat, limiting the maximum thermodynamic efficiency of a standard photovoltaic device to 32%. Multiple exciton generation (MEG) provides a potential route to increase solar cell efficiencies by creating multiple charge carriers from a single photon absorption.[2,3] The multiple electron−hole pairs are produced when a highly excited charge carrier relaxes to the band edge while exciting another electron across the band gap. MEG yields in quantum dots (QDs) are higher than those in bulk semiconductors[2−25] because a momentum conservation requirement at a second exciton generation is lifted in QDs, and Coulomb interactions between electrons and holes are enhanced due to closer proximity of the charge carriers. Even photon-to-current efficiency exceeding 100% was recently observed, demonstrating the ability of QDs as solar cells.[3] On the contrary, Auger recombination (AR), in which a ME annihilates to a single exciton (SE) of high energy, reduces photovoltaic efficiencies by accelerating energy losses to heat.[7,12,26−30]

An AR rate in bulk has an activation threshold that arises from a requirement of energy and translational momentum conservation during annihilation of a ME, exhibiting the simple Arrhenius-type rate, $\exp(-\gamma E_g/k_B T)$ with the band gap energy E_g, temperature T, and the Boltzmann constant k_B.[31,32] γ is a constant dependent on the electronic structure. Compared to mature experimental and theoretical treatments of bulk crystals contributed by the condensed matter physics community,[33,34] studies for temperature dependence of QD properties have been much less established, and thus the temperature dependence has received much recent attention.[35−37] A lowest excitation energy, E_g, was measured for various QDs over wide

Received: October 25, 2013
Accepted: December 9, 2013
Published: December 12, 2013

 © 2013 American Chemical Society

temperature ranges, reporting the linear temperature dependence.[38−40] Also, dephasing dynamics of coherent SEs and MEs in QDs under some temperatures was theoretically discussed with roles of the phonon modes.[39,41]

The temperature dependence of the MEG and AR provides significant information on physical properties of the Auger dynamics. The barrierless MEG and AR, which have moderate or no temperature dependence, directly indicate that momenta of carriers are not conserved in QDs since the momentum conservation directly results in the Arrhenius-type Auger dynamics.[42−44] It has been theoretically and experimentally reported that the barrierless AR is dominant in QDs, and its rate should be independent of temperature.[42−45] However, there has been no direct evidence to prove the temperature independence, and its physical origin is only poorly understood. Kobayashi and Tamai recently observed the logarithmic temperature dependence of the AR rates in CdTe QDs.[45] The logarithmic temperature dependence is quite different from the usual Arrhenius-type dependence. Although they did not discuss any physical origin of the temperature dependence, this anomalous temperature dependence of the Auger rates implies a new physical mechanism of the Auger processes.

In order to elucidate their physical origins, it is important how the anomalous Auger dynamics are induced in the QDs. This theoretical study focuses on explicit temperature dependence of the MEG and AR dynamics in the two representative QDs, $Si_{29}H_{24}$ and $Cd_{33}Se_{33}$, for the various temperatures T = 10, 50, 100, 200, and 300 K. We will rationalize the anomalous temperature dependence from the viewpoint of the phonon dynamics and its coupling to carriers in the QDs, concluding that the Auger processes in a QD are induced by the electron−phonon couplings.

Each panel of Figure 1 shows the single exciton (SE) and double exciton (DE) density of states (DOS) of the two QDs for 10 and 300 K. The other DOS for T = 50, 100, and 200 K is shown in ref 46. The underlying atomic structure, thermal fluctuations, and Coulomb interactions break electronic state degeneracies, leading to the complicated multilevel band structures of the QDs.[11] The resulting DOS is thus quasi-continuous for all the shown QDs and temperatures. The temperature effect on the DOS is not significant. Since the QD size of $Cd_{33}Se_{33}$ is larger than the size of $Si_{29}H_{24}$, the former gives the smaller energy gap E_g, and the DOS is higher and smoother in the former than in the latter. The DE DOS shown by the green lines starts at higher energies than the SE DOS. However, because the combinatorial number of DEs grows significantly faster with energy than the number of SEs, the DE DOS completely dominates over the SE DOS at higher energies. The ratio of the DE DOS over the SE DOS is higher with $Cd_{33}Se_{33}$ at high energies, implying its faster MEG than the MEG in $Si_{29}H_{24}$. The negative linear temperature dependence of E_g from 10 to 300 K is shown in Figure S1(B) of ref 46, where the band gaps change by 0.35 eV for $Si_{29}H_{24}$ and by 0.20 eV for $Cd_{33}Se_{33}$.

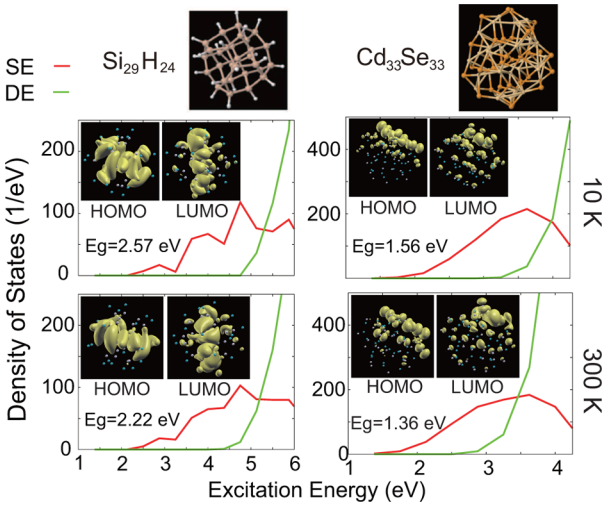

Figure 1. Geometrical and electronic structures of $Si_{29}H_{24}$ and $Cd_{33}Se_{33}$. $Si_{29}H_{24}$ is passivated by hydrogen atoms to avoid dangling bonds on the QD surface. Each panel shows DOS for $Si_{29}H_{24}$ and $Cd_{33}Se_{33}$ at 10 and 300 K. Higher temperatures give smaller band gaps reflecting enhanced thermal fluctuations at the high temperature. The inserts in each panel show the corresponding HOMO and LUMO orbitals.

Diameters of the two representative QDs, $Si_{29}H_{24}$ and $Cd_{33}Se_{33}$, which we will study are approximately 0.7 and 1.6 nm, respectively. The QD structures drawn in Figure 1 are snapshots from the dynamics simulation at 300 K. No drastic structural change was observed during the dynamics simulations. The hydrogen ligands of $Si_{29}H_{24}$ effectively eliminate dangling bonds on the bare QD surface and avoid surface defects.[29] As a result, the HOMO and LUMO orbitals of $Si_{29}H_{24}$ exist inside the QD core. On the other hand, the HOMO and LUMO orbitals of $Cd_{33}Se_{33}$ without a surface passivation appear notably localized on the surface due to the surface defects. The temperature effect on the HOMO and LUMO orbitals is not significant in both QDs; the HOMO and LUMO orbitals of the two QDs are similar at 10 and 300 K.

Figure 2 describes relaxation of total SE population started from an initially excited SE state which has the displayed energy. The decay of the total population of all SEs directly reflects the MEG since the initial SE state couples to DE states as well as to other SE states. Our simulation includes SEs, DEs and the ground state, and the ground state population remains negligible throughout the simulation up to 10 ps, which is in agreement with the experiments.[47−49] The MEG dynamics starts to follow an exponential decay as the number of quantum states involved in the MEG becomes statistically enough. The exponential MEG time scales, τ_e, are displayed in Figure 2. The MEG dynamics is strongly influenced by the temperature both in $Si_{29}H_{24}$ and $Cd_{33}Se_{33}$. Additionally, in spite of the higher DE/SE DOS ratio of $Cd_{33}Se_{33}$ than $Si_{29}H_{24}$, the MEG time scales of the former are longer than the time scales of the latter. These facts cannot be explained by the little difference in the excitation energies displayed in each case of Figure 2.

We introduce the MEG rates by inverses of the MEG time scales obtained above and plot the rates for $Si_{29}H_{24}$ and $Cd_{33}Se_{33}$ as a function of temperature T in the upper panel of Figure 3. The MEG rates exhibit the linear relationships with $\ln(T/T_0)$, which agrees with the experimental AR rates shown in the insert.[45] As the data in Figure 3 indicate, the scaling factor T_0 is 1 K. Since both of the MEG and AR occur through the same mechanism, i.e., the nonadiabatic(NA) couplings, the similar temperature dependence should be reproduced. In addition, the AR follows the preceding MEG;[13,50] the MEG prepares initial DE states for the AR and provides the similar temperature dependence through the initial conditions. The $\ln(T/T_0)$ dependence means that, while the change of the Auger rates in the higher temperature range is moderate, the rates drastically decrease in the lower temperature range. Such

dx.doi.org/10.1021/jz402305r | J. Phys. Chem. Lett. 2014, 5, 99−105

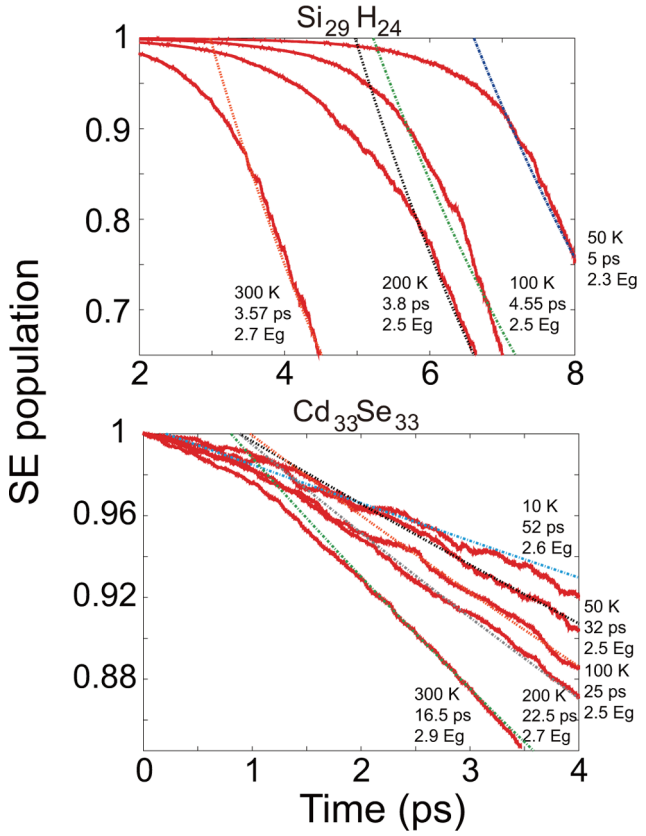

Figure 2. Relaxation dynamics of total SE population started from an initially excited SE state with the shown temperatures and excitation energies. All the relaxation dynamics exhibit an exponential decay at the later stage. The exponential time scales, τ_e, are displayed. The MEG significantly depends on the temperature.

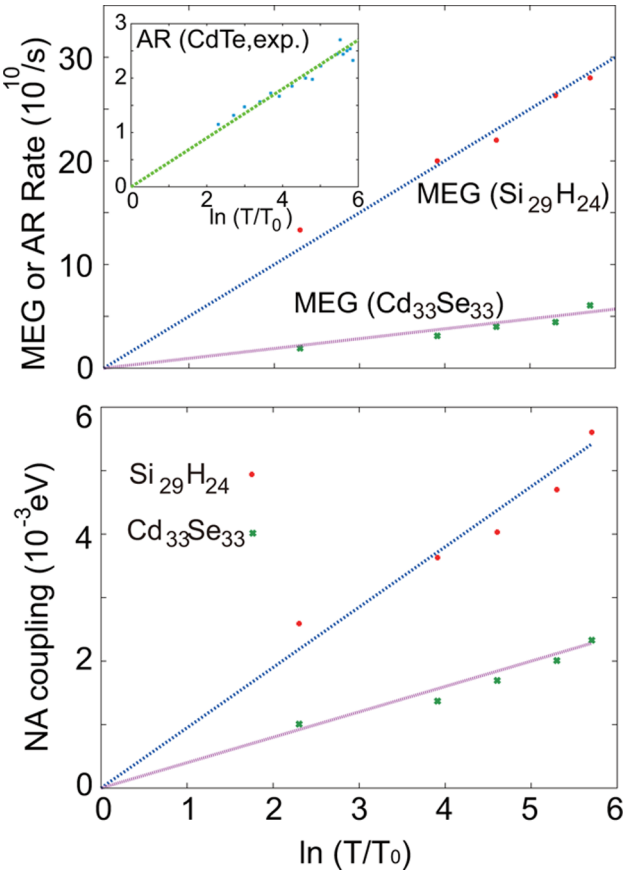

Figure 3. (top) MEG and AR rates as a function of temperature. The experimental AR data shown in the insert were observed in ref 45. The gradients are 5, 0.95, and 0.45 for the $Si_{29}H_{24}$, $Cd_{33}Se_{33}$, and experimental CdTe QD of 4 nm, respectively. All the Auger rates are linearly proportional to $\ln(T/T_0)$. (bottom) Averaged absolute values of NA coupling strength as a function of temperature. The NA couplings show the same temperature dependence, $\ln(T/T_0)$. The gradients are 9.5×10^{-4} and 4.0×10^{-4} for $Si_{29}H_{24}$ and $Cd_{33}Se_{33}$, respectively.

Auger dynamics cannot be predicted only by the static electronic structure like, E_g which has the simple linear dependence on the temperature and the DOS of the QDs which has the similar shape almost independent of the temperature. The previous experiments also revealed that the Auger dynamics in a QD is insensitive to E_g in contrast with bulk semiconductors where the Arrhenius-type rate of the Auger dynamics changes by 5 orders of magnitude per 1 eV variation of E_g.[31,42] The current MEG time scales, which cannot be attributed to the E_g, are in harmony with these previous experimental observations.[42,45]

Reproducing $\ln(T/T_0)$ dependence of the Auger rates observed in the experiments directly demonstrates that the Arrhenius-type threshold reported in bulk semiconductors is no longer valid for the MEG and AR in the small QDs, and therefore the momentum conservation is not required for carriers involved in their MEG and AR.[42−44] Our simulation is based on the adiabatic picture where transitions between states are caused by the NA electron−phonon coupling; the NA electron−phonon coupling is the main interaction to cause the Auger dynamics in the current method. Thus, the same temperature dependence of the Auger rates found in the experiment and our simulation strongly suggests that the NA electron−phonon coupling is the important mechanism of the Auger dynamics in real QDs.

We give quantitative analyses on the NA electron−phonon couplings in the lower panel of Figure 3. The lower panel plots averaged absolute strength of the NA phonon couplings as a function of temperature. The calculated NA phonon couplings exhibit the linear relationships with $\ln(T/T_0)$ both in $Si_{29}H_{24}$ and $Cd_{33}Se_{33}$. The NA couplings do not significantly change at the higher temperature, while they become drastically weakened at the lower temperature. This $\ln(T/T_0)$ dependence of the NA phonon couplings is directly related to the $\ln(T/T_0)$ dependence in the Auger rates, leading to the important conclusion that the Auger processes are actually induced by the NA electron−phonon couplings. The above findings are the first direct evidence that the MEG and AR in semiconductor QDs are phonon-assisted.

The gradients of the linear lines in Figure 3 are to be determined by intrinsic properties of the QDs related to the NA phonon couplings, e.g., a ratio of a surface to volume, surface passivation, phonon frequencies and charge distribution. In fact, the following three factors can lead to the larger gradients in $Si_{29}H_{24}$; the hydrogen surface passivation inducing the high-frequency and broad phonon modes, the delocalized charge density effectively coupling to the many phonon modes, and the large surface ratio enhancing the effect of the surface ligand modes.

Our real-time simulation method explicitly includes the phonon dynamics and can provide a phonon mode analysis.

dx.doi.org/10.1021/jz402305r | J. Phys. Chem. Lett. 2014, 5, 99−105

Fourier transforms of fluctuations in energy gaps between SE and DE states along a nuclear trajectory identify the frequencies of the phonons that couple to the Auger dynamics. Figure 4

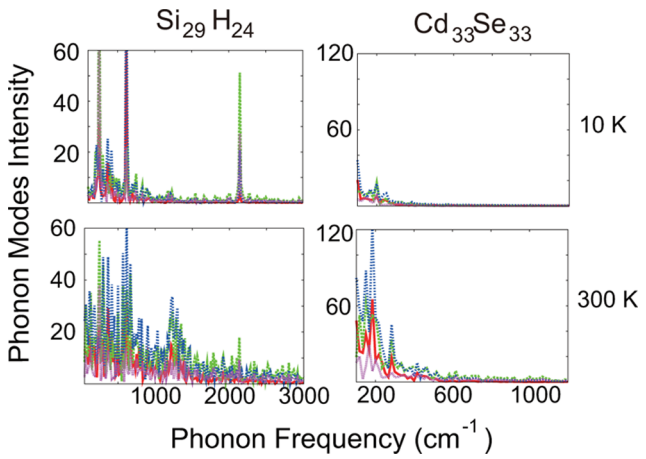

Figure 4. Spectral density of phonon modes included in $Si_{29}H_{24}$ and $Cd_{33}Se_{33}$. $Si_{29}H_{24}$ exhibits the broader phonon modes due to the surface hydrogen ligands. The spectral density at 300 K has broader phonon frequency. The spectral density shrinks and becomes narrower at 10 K both in $Si_{29}H_{24}$ and $Cd_{33}Se_{33}$, indicating the frozen phonon dynamics.

shows the phonon spectral density involved in the MEG and AR dynamics. The other phonon spectra at T = 50, 100, and 200 K are shown in ref 46. In all the panels, the red, green, blue, and pink lines correspond to the SE and DE pairs of lowest-energy SE and lowest-energy DE, lowest-energy SE and higher-energy DE, higher-energy SE and lowest-energy DE, and higher-energy SE and higher-energy DE, respectively. The phonon modes appearing in the spectral density are largely related to the MEG and AR, although it is not straightforward to distinguish phonon modes involved in elastic and inelastic scatterings as well as acoustic and optical phonon modes. The NA coupling appearing in eq 3 to cause the MEG and AR is calculated by time-dependent fluctuations of each state basis as in eq 4, which is essentially correlated to time-dependent fluctuations of eigen energy of each state. The spectral density shown in Figure 4 corresponds to the latter fluctuations. In fact, we have successfully analyzed such spectral density to characterize the MEG and AR dynamics at the ambient temperature.[12,13,50] Additionally, it can be easily assumed that the temperature dependences of phonon modes involved in elastic and inelastic scatterings are similar to each other and do not differ qualitatively.

$Si_{29}H_{24}$ at 300 K exhibits a broad and high-frequency phonon spectrum caused by the larger thermal fluctuations. The NA couplings proportional to the nuclear velocity as in eq 4 are enhanced with the higher-frequency phonon modes. On the other hand, the phonon spectrum at 10 K drastically shrinks and exhibits narrower peaks, indicating that the phonon mode dynamics becomes frozen and inactive. This disappearance of phonon modes rationalizes the observed sharp decrease in the Auger rates at the lower temperature in Figure 3.

The high-frequency peak around 2000 cm^{-1} corresponds to the Si−H ligand modes. The surface passivation of $Si_{29}H_{24}$ provides the high-frequency and broad phonon modes, which play a key role in the Auger dynamics.[12,13,50] The phonon spectra of $Cd_{33}Se_{33}$ have only the lower-frequency peaks due to the heavier masses of Cd and Se atoms as well as no passivation. In addition, the bare QD surface has defects and the charge is localized on the $Cd_{33}Se_{33}$ surface as shown in Figure 1, indicating the poor coupling of carries with the phonon modes. The poor couplings and the lower-frequency phonon modes both cause the weaker NA electron−phonon couplings in $Cd_{33}Se_{33}$. The smaller MEG rates for $Cd_{33}Se_{33}$ compared to $Si_{29}H_{24}$ in spite of the higher ratio of the DE/SE DOS of the former are essentially rationalized by the weaker NA phonon couplings. The surface structure and ligand identity strongly affect the NA phonon couplings and thus the Auger dynamics.

The ligand contribution to the QD electronic states and the Auger dynamics decreases with increasing the QD size, reflecting the reduced surface-to-volume ratio. The size dependence of the AR time has been experimentally suggested.[24,28,30] Such size scaling allows the direct comparison of our theoretical results with the experimental data, and the good agreement in the AR time was already reported.[13] This agreement indicates an important fact that our QDs still maintain the similar Auger dynamics properties to those of larger QDs, and can be discussed in the same line of experimental QDs; the qualitative results we reported here would not be changed even in larger QDs. The similar temperature dependence for the different QDs we demonstrated also suggests material independence and universality of the Auger dynamics in nanoscale QDs.

In conclusion, we found and rationalized the new type of Auger processes in the representative QDs through the time-domain, atomistic, *ab initio* simulations. The calculated $\ln(T/T_0)$ dependence of the Auger rates is qualitatively different from the simple Arrhenius-type threshold reported in bulk semiconductors, but well explains the experimental observation in the CdTe QD. We for the first time elucidated the physical origin of the $\ln(T/T_0)$ dependence, and indicated that the $\ln(T/T_0)$ dependence stems from the same temperature dependence of the NA phonon couplings. These findings are the first direct evidence that the Auger processes are caused by the NA electron−phonon couplings. The physical insights obtained in this study suggest that effective Auger dynamics can be achieved by providing high-frequency and broad phonon modes and a charge distribution delocalized over a QD. Manipulation of temperature, defects, and surface passivations for controlling phonon dynamics will play a pivotal role to enhance or suppress MEG and AR processes.

■ COMPUTATIONAL METHODS

The current non-Born−Oppenheimer (non-BO) Auger dynamics involving SE and DE states are simulated based on the time-domain density functional theory (TDDFT) formulated in adiabatic Kohn−Sham (KS) bases.[12,13,50] Transitions between different SE and/or DE states occur due to the NA couplings. The adiabatic representation of the Auger dynamics differs from the diabatic picture where the Auger dynamics is caused by Coulomb interactions between electrons and holes explicitly appearing in the off-diagonal part of the Hamiltonian. The adiabatic representation includes such Coulomb coupling only implicitly in the Hamiltonian. All Coulomb couplings are diagonalized out in the adiabatic Hamiltonian; the electron−hole interaction is partly taken into account through an exchange-correlation function of the DFT.

Electronic structures and adiabatic molecular dynamics (MD) are computed with VASP using a converged plane-

dx.doi.org/10.1021/jz402305r | J. Phys. Chem. Lett. 2014, 5, 99−105

wave basis. QDs are placed periodically in a cubic simulation cell. At least 8 Å of vacuum is set between QD replicas to prevent spurious interactions of periodic QD images. The Perdew–Wang-91 (PW91) generalized gradient density functional and projector-augmented-wave pseudopotentials are used. The QD geometry is initially generated from the corresponding bulk structure. The Si QD is further passivated by hydrogen atoms to generate high-frequency phonon mods. The crystal QDs are then fully optimized at zero temperature and heated up to an ambient temperature by repeated velocity rescaling. Microcanonical trajectories of 5 to 10 ps are calculated by the ground electronic state *ab initio* MD with a 1 fs time-step.

Our formulation for the MEG and AR dynamics is based on the second quantization including the ground, SE and DE states, $|\Phi_g(\mathbf{r};\mathbf{R})\rangle$, $|\Phi_{SE}^{i,j}(\mathbf{r};\mathbf{R})\rangle$, and $|\Phi_{DE}^{i,j,k,l}(\mathbf{r};\mathbf{R})\rangle$, respectively. Bases for SEs and DEs are defined as

$$|\Phi_{SE}^{i,j}\rangle = \hat{a}_i^\dagger \hat{a}_j |\Phi_g\rangle, \qquad |\Phi_{DE}^{i,j,k,l}\rangle = \hat{a}_i^\dagger \hat{a}_j \hat{a}_k^\dagger \hat{a}_l |\Phi_g\rangle \tag{1}$$

where the electron creation and annihilation operators, $\hat{a}_i^\dagger$ and $\hat{a}_j$, generate and annihilate an electron in the ith and jth adiabatic KS orbitals, respectively. The total wave function is then expanded as

$$|\Psi(t)\rangle = C_g(t)|\Phi_g\rangle + \sum_{i,j} C_{SE}^{i,j}(t)|\Phi_{SE}^{i,j}\rangle + \sum_{i,j,k,l} C_{DE}^{i,j,k,l}(t)|\Phi_{DE}^{i,j,k,l}\rangle \tag{2}$$

Substitution of eq 2 into the time-dependent Schrödinger equation leads to the equations of motion for the expansion coefficients in eq 2:

$$i\hbar\frac{\partial C_X(t)}{\partial t} = C_X(t)E_X - i\hbar C_g(t)\mathbf{d}_{X;g}\cdot\dot{\mathbf{R}} - i\hbar\sum_{i',j'} C_{SE}^{i',j'}(t)\mathbf{d}_{X;SE,i',j'}\cdot\dot{\mathbf{R}} - i\hbar\sum_{i',j',k',l'} C_{DE}^{i',j',k',l'}(t)\mathbf{d}_{X;DE,i',j',k',l'}\cdot\dot{\mathbf{R}} \tag{3}$$

where X and Y now correspond to either ground, SE, or DE state, E_X is the state energy, and the NA couplings are introduced by

$$\mathbf{d}_{X;Y}\cdot\dot{\mathbf{R}} \equiv \langle\Phi_X|\nabla_{\mathbf{R}}|\Phi_Y\rangle\cdot\dot{\mathbf{R}} = \langle\Phi_X|\frac{\partial}{\partial t}|\Phi_Y\rangle \tag{4}$$

which cause NA transitions from each of the ground, SE, and DE states to another state. This NA phonon coupling stems from the dependence of the adiabatic KS orbitals on the phonon dynamics $\mathbf{R}(t)$. Since the NA coupling is proportional to the nuclear velocity $\dot{\mathbf{R}}$, NA transitions would never happen under the BO approximation. The atomistic simulations of the MEG and AR dynamics are performed by directly solving the equations of motion eq 3 with the time-dependent NA couplings and band energies obtained by the *ab initio* MD simulations.[12,13,50]

The simulations are extremely large-scale; the 24 CB and 25 VB orbitals used in our calculations on the $Si_{29}H_{24}$ QD give rise to 600 SE and 97 500 DE states. The total number of states is 98 101, and the Hamiltonian appearing in the time-dependent Schrödinger equation, eq 3, contains $98\,101^2 = 9\,623\,806\,201$ matrix elements. However, the Hamiltonian is sparse since the NA couplings in eq 4 connect KS basis states that differ only in a single electron or hole.[12,50] Based on this physical fact, we developed the efficient simulation code that can remove all the zero components from the sparse matrix, and solve eq 3 using only the extracted nonzero parts of the Hamiltonian.[12]

Our Auger dynamics simulation simultaneously calculates the MEG and AR, and can discuss interplay between them. All the NA couplings are treated nonperturbatively, and our results exhibit not only simple exponential but also more complicated Auger dynamics. Our real-time simulation explicitly includes phonon dynamics, and can discuss temperature effects accounting for fluctuations of the band energies and NA couplings without any prepared modeling. We define the temperature through mean squares of microscopic phonon velocities. Phonon dynamics is actually influenced by the temperature as were reflected in temperature-dependent linewidths of fluorescence spectra[35,51] and in a dephasing process related to ME fission depending on the temperature.[39,41]

■ ASSOCIATED CONTENT

Supporting Information

Detailed data of Figures 1 and 4. This material is available free of charge via the Internet at http://pubs.acs.org.

■ AUTHOR INFORMATION

Corresponding Author

*E-mail: kim@kuchem.kyoto-u.ac.jp; phone: +81 (75) 753 4021; fax: +81 (75) 753 4000.

Notes

The authors declare no competing financial interest.

■ ACKNOWLEDGMENTS

K.H.D. appreciates Dr. Oleg V. Prezhdo for fruitful discussions. K.H.D. acknowledges the financial support from JST (PRESTO), and Grant-in-Aids for Scientific Research from the Japan Society for the Promotion of Science (KAKENHI), Grant No. 24750016. N.T. acknowledges the KAKENHI, Grant No. 22350012.

■ REFERENCES

(1) Nozik, A. J. Spectroscopy and Hot Electron Relaxation Dynamics in Semiconductor Quantum Wells and Quantum Dots. *Annu. Rev. Phys. Chem.* **2001**, *52*, 193–231.

(2) McGuire, J. A.; Joo, J.; Pietryga, J. M.; Schaller, R. D.; Klimov, V. I. New Aspects of Carrier Multiplication in Semiconductor Nanocrystals. *Acc. Chem. Res.* **2008**, *41*, 1810–1819.

(3) Semonin, O. E.; Luther, J. M.; Choi, S.; Chen, H.-Y.; Gao, J.; Nozik, A. J.; Beard, M. C. Peak External Photocurrent Quantum Efficiency Exceeding 100% via MEG in a Quantum Dot Solar Cell. *Science* **2011**, *334*, 1530–1533.

(4) Beard, M. C.; Knutsen, K. P.; Yu, P. R.; Luther, J. M.; Song, Q.; Metzger, W. K.; Ellingson, R. J.; Nozik, A. J. Multiple Exciton Generation in Colloidal Silicon Nanocrystals. *Nano Lett.* **2007**, *7*, 2506–2512.

(5) Beard, M. C.; Midgett, A. G.; Hanna, M. C.; Luther, J. M.; Hughes, B. K.; Nozik, A. J. Comparing Multiple Exciton Generation in Quantum Dots to Impact Ionization in Bulk Semiconductors: Implications for Enhancement of Solar Energy Conversion. *Nano Lett.* **2010**, *10*, 3019–3027.

(6) Beard, M. C.; Midgett, A. G.; Law, M.; Semonin, O. E.; Ellingson, R. J.; Nozik, A. J. Variations in the Quantum Efficiency of Multiple Exciton Generation for a Series of Chemically Treated PbSe Nanocrystal Films. *Nano Lett.* **2009**, *9*, 836–845.

(7) Califano, M. Direct and Inverse Auger Processes in InAs Nanocrystals: Can the Decay Signature of a Trion Be Mistaken for Carrier Multiplication? *ACS Nano* **2009**, *3*, 2706−2714.
(8) Califano, M. Photoinduced Surface Trapping and the Observed Carrier Multiplication Yields in Static CdSe Nanocrystal Samples. *ACS Nano* **2011**, *5*, 3614−3621.
(9) Ellingson, R. J.; Beard, M. C.; Johnson, J. C.; Yu, P. R.; Micic, O. I.; Nozik, A. J.; Shabaev, A.; Efros, A. L. Highly Efficient Multiple Exciton Generation in Colloidal PbSe and PbS Quantum Dots. *Nano Lett.* **2005**, *5*, 865−871.
(10) Fischer, S. A.; Isborn, C. M.; Prezhdo, O. V. Excited States and Optical Absorption of Small Semiconducting Clusters: Dopants, Defects and Charging. *Chem. Sci.* **2011**, *2*, 400−406.
(11) Franceschetti, A.; An, J. M.; Zunger, A. Impact Ionization Can Explain Carrier Multiplication in PbSe Quantum Dots. *Nano Lett.* **2006**, *6*, 2191−2195.
(12) Hyeon-Deuk, K.; Prezhdo, O. V. Time-Domain *ab initio* Study of Auger and Phonon-Assisted Auger Processes in a Semiconductor Quantum Dot. *Nano Lett.* **2011**, *11*, 1845−1850.
(13) Hyeon-Deuk, K.; Prezhdo, O. V. Multiple Exciton Generation and Recombination Dynamics in Small Si and CdSe Quantum Dots: An *ab initio* Time-Domain Study. *ACS Nano* **2012**, *6*, 1239−1250.
(14) Isborn, C. M.; Kilina, S. V.; Li, X. S.; Prezhdo, O. V. Generation of Multiple Excitons in PbSe and CdSe Quantum Dots by Direct Photoexcitation: First-Principles Calculations on Small PbSe and CdSe Clusters. *J. Phys. Chem. C* **2008**, *112*, 18291−18294.
(15) Ji, M.; Park, S.; Connor, S. T.; Mokari, T.; Cui, Y.; Gaffney, K. J. Efficient Multiple Exciton Generation Observed in Colloidal PbSe Quantum Dots with Temporally and Spectrally Resolved Intraband Excitation. *Nano Lett.* **2009**, *9*, 1217−1222.
(16) Klimov, V. I.; Mikhailovsky, A. A.; McBranch, D. W.; Leatherdale, C. A.; Bawendi, M. G. Quantization of Multiparticle Auger Rates in Semiconductor Quantum Dots. *Science* **2000**, *287*, 1011−1013.
(17) Kobayashi, Y.; Udagawa, T.; Tamai, N. Carrier Multiplication in CdTe Quantum Dots by Single-Photon Timing Spectroscopy. *Chem. Lett.* **2009**, *38*, 830−831.
(18) Luo, J. W.; Franceschetti, A.; Zunger, A. Carrier Multiplication in Semiconductor Nanocrystals: Theoretical Screening of Candidate Materials Based on Band-Structure Effects. *Nano Lett.* **2008**, *8*, 3174−3181.
(19) Murphy, J. E.; Beard, M. C.; Norman, A. G.; Ahrenkiel, S. P.; Johnson, J. C.; Yu, P.; Micic, O. I.; Ellingson, R. J.; Nozik, A. J. PbTe Colloidal Nanocrystals: Synthesis, Characterization, and Multiple Exction Generation. *J. Am. Chem. Soc.* **2006**, *128*, 3241−3247.
(20) Piryatinski, A.; Velizhanin, K. A. An Exciton Scattering Model for Carrier Multiplication in Semiconductor Nanocrystals: Theory. *J. Chem. Phys.* **2010**, *133*, 084508-1−084508-19.
(21) Rabani, E.; Baer, R. Distribution of Multiexciton Generation Rates in CdSe and InAs Nanocrystals. *Nano Lett.* **2008**, *8*, 4488−4492.
(22) Rabani, E.; Baer, R. Theory of Multiexciton Generation in Semiconductor Nanocrystals. *Chem. Phys. Lett.* **2010**, *496*, 227−235.
(23) Schaller, R. D.; Klimov, V. I. High Efficiency Carrier Multiplication in PbSe Nanocrystals: Implications for Solar Energy Conversion. *Phys. Rev. Lett.* **2004**, *92*, 186601-1−186601-4.
(24) Schaller, R. D.; Pietryga, J. M.; Klimov, V. I. Carrier Multiplication in InAs Nanocrystal Quantum Dots with an Onset Defined by the Energy Conservation Limit. *Nano Lett.* **2007**, *7*, 3469−3476.
(25) Schaller, R. D.; Agranovich, V. M.; Klimov, V. I. High-Efficiency Carrier Multiplication Through Direct Photogeneration of Multi-Excitons via Virtual Single-Exciton States. *Nat. Phys.* **2005**, *1*, 189−194.
(26) Huang, L. B.; Krauss, T. D. Quantized Bimolecular Auger Recombination of Excitons in Single-Walled Carbon Nanotubes. *Phys. Rev. Lett.* **2006**, *96*, 057407-1−057407-4.
(27) Hyeon-Deuk, K.; Prezhdo, O. V. Symmetric Band Structures and Asymmetric Ultrafast Electron and Hole Relaxations in Silicon and Germanium Quantum Dots: Time-Domain *ab initio* Simulation. *Dalton Trans.* **2009**, *45*, 10069−10077.
(28) Kobayashi, Y.; Nishimura, T.; Yamaguchi, H.; Tamai, N. Effect of Surface Defects on Auger Recombination in Colloidal CdS Quantum Dots. *J. Phys. Chem. Lett.* **2011**, *2*, 1051−1055.
(29) Kobayashi, Y.; Pan, L.; Tamai, N. Effects of Size and Capping Reagents on Biexciton Auger Recombination Dynamics of CdTe Quantum Dots. *J. Phys. Chem. C* **2009**, *113*, 11783−11789.
(30) Robel, I.; Gresback, R.; Kortshagen, U.; Schaller, R. D.; Klimov, V. I. Universal Size-Dependent Trend in Auger Recombination in Direct-Gap and Indirect-Gap Semiconductor Nanocrystals. *Phys. Rev. Lett.* **2009**, *102*, 177404-1−177404-4.
(31) Beattie, A. R.; Landsberg, P. T. Auger Effect in Semiconductors. *Proc. R. Soc. London A* **1959**, *249*, 16−29.
(32) Haug, A. Band-to-Band Auger Recombination in Semiconductors. *J. Phys. Chem. Sol.*. **1988**, *49*, 599−605.
(33) Shim, Y.; Aoh, H.; Sakamoto, J.; Wakita, K.; Mamedov, N. Temperature Dependence of Dielectric Function and Optical Transitions in $TlInSe_2$ and $TlGaTe_2$. *Thin Solid Films* **2011**, *519*, 2852−2854.
(34) Shim, Y.; Nishimoto, Y.; Okada, W.; Wakita, K.; Mamedov, N. Temperature-Dependent Spectro-Ellipsometric Studies of Optical Transitions Near Absorption Edge of $TlInS_2$. *Phys. Status Solidi* **2008**, *5*, 1121−1124.
(35) Kim, D.; Mishima, T.; Tomihira, K.; Nakayama, M. Temperature Dependence of Photoluminescence Dynamics in Colloidal CdS Quantum Dots. *J. Phys. Chem. C* **2008**, *112*, 10668−10673.
(36) Kim, D.; Okahara, S.; Nakayama, M. Experimental Verification of Forster Energy Transfer Between Semiconductor Quantum Dots. *Phys. Rev. B* **2008**, *78*, 153301-1−153301-4.
(37) Kim, D.; Okazaki, K.; Nakayama, M. Temperature Dependence of the Energy Transfer of Exciton States in Bilayer Structures of CdSe/ZnS Quantum Dots. *Phys. Rev. B* **2009**, *80*, 045322−1−045322−5.
(38) Fernee, M. J.; Jensen, P.; Rubinsztein-Dunlop, H. Origin of the Large Homogeneous Line Widths Obtained from Strongly Quantum Confined PbS Nanocrystals at Room Temperature. *J. Phys. Chem. C* **2007**, *111*, 4984−4989.
(39) Kamisaka, H.; Kilina, S. V.; Yamashita, K.; Prezhdo, O. V. *Ab initio* Study of Temperature- and Pressure Dependence of Energy and Phonon-Induced Dephasing of Electronic Excitations in CdSe and PbSe Quantum Dots. *J. Phys. Chem. C* **2008**, *112*, 7800−7808.
(40) Olkhovets, A.; Hsu, R.-C.; Lipovskii, A.; Wise, F. W. Size-Dependent Temperature Variation of the Energy Gap in Lead-Salt Quantum Dots. *Phys. Rev. Lett.* **1998**, *81*, 3539−3542.
(41) Madrid, A. B.; Hyeon-Deuk, K.; Prezhdo, O. V. Phonon-Induced Dephasing of Excitons in Semiconductor Quantum Dots: Multiple Exciton Generation, Fission, and Luminescence. *ACS Nano* **2009**, *3*, 2487−2494.
(42) Pietryga, J. M.; Zhuravlev, K. K.; Whitehead, M.; Klimov, V. I.; Schaller, R. D. Evidence for Barrierless Auger Recombination in PbSe Nanocrystals: A Pressure-Dependent Study of Transient Optical Absorption. *Phys. Rev. Lett.* **2008**, *101*, 217401-1−217401-4.
(43) Kharchenko, V.; Rosen, M. Auger Relaxation Processes in Semiconductor Nanocrystals and Quantum Wells. *J. Lumin.* **1996**, *70*, 158−169.
(44) Zegrya, G. G.; Samosvat, D. M. Mechanisms of Auger Recombination in Semiconducting Quantum Dots. *J. Exp. Theor. Phys.* **2001**, *104*, 951−965.
(45) Kobayashi, Y.; Tamai, N. Size-Dependent Multiexciton Spectroscopy and Moderate Temperature Dependence of Biexciton Auger Recombination in Colloidal CdTe Quantum Dots. *J. Phys. Chem. C* **2010**, *114*, 17550−17556.
(46) See Supporting Information for the detailed data of Figures 1 and 4.
(47) Nirmal, M.; Dabbousi, B. O.; Bawendi, M. G.; Macklin, J. J.; Trautman, J. K.; Harris, T. D.; Brus, L. E. Fluorescence Intermittency in Single Cadmium Selenide Nanocrystals. *Nature* **1996**, *383*, 802−804.

(48) Peterson, J. J.; Krauss, T. D. Fluorescence Spectroscopy of Single Lead Sulfide Quantum Dots. *Nano Lett.* **2006**, *6*, 510−514.
(49) Sykora, M.; Mangolini, L.; Schaller, R. D.; Kortshagen, U.; Jurbergs, D.; Klimov, V. I. Size-Dependent Intrinsic Radiative Decay Rates of Silicon Nanocrystals at Large Confinement Energies. *Phys. Rev. Lett.* **2008**, *100*, 067401-1−067401-4.
(50) Hyeon-Deuk, K.; Prezhdo, O. V. Photoexcited Electron and Hole Dynamics in Semiconductor Quantum Dots: Phonon-Induced Relaxation, Dephasing, Multiple Exciton Generation and Recombination. *J. Phys.: Condens. Matter* **2012**, *24*, 363201-1−363201-12.
(51) Sychugov, I.; Juhasz, R.; Valenta, J.; Linnros, J. Narrow Luminescence Linewidth of a Silicon Quantum Dot. *Phys. Rev. Lett.* **2005**, *94*, 087405-1−087405-4.